Rev.Adv.Mater.Sci. 5 (2003) 76-81

SURFACE SPIN DISORDER AND EXCHANGE BIAS IN $La_{0.7}Ca_{0.3}MnO_3$ NANOPARTICLES SYNTHESISED BY MECHANOCHEMICAL PROCESSING

M. Muroi [1], P. G. McCormick [1] and R. Street [2]

[1] Advanced Nano Technologies, 112 Radium Street, Welshpool, WA 6106, Australia
[2] Department of Physics, The University of Western Australia, 35 Stirling Highway, Crawley, WA 6009, Australia

Rreceived: June 24, 2003

Abstract. Nanoparticles of $La_{0.7}Ca_{0.3}MnO_3$ have been synthesised via the chemical reaction $0.7LaCl_3 + 0.3CaCl_2 + MnCl_2 + 2.35Na_2CO_3 + 0.325O_2 \rightarrow La_{0.7}Ca_{0.3}MnO_3 + 4.7NaCl + 2.35CO_2$ effected by high-energy ball milling and subsequent heat treatment. Single-phase $La_{0.7}Ca_{0.3}MnO_3$ particles having crystallite sizes ranging between 24 nm and 1 μm were obtained after removing the NaCl by-product phase by washing. Magnetic measurements showed that the spontaneous magnetisation decreased with deceasing crystallite size; that the coercivity increased with decreasing temperature; and that below about 50K field-cooled hysteresis loops for the smallest particles were shifted towards the negative field. These observations are discussed in terms of a model in which it is assumed that each crystallite consists of a ferromagnetic core and a spin-glass shell that are exchange-coupled.

1. INTRODUCTION

Nanoparticles of magnetic materials have recently been the subject of intense research from both scientific and technological points of view. On the one hand, nanoparticles often exhibit magnetic properties that differ, sometimes qualitatively, from those of their bulk counterparts; it is of fundamental importance to elucidate the differences. On the other hand, magnetic nanoparticles have great potential for use in a wide range of applications, including magnetic-recording media, sensors, permanent magnets and ferrofluids. In this work we have synthesised nanoparticles of $La_{0.7}Ca_{0.3}MnO_3$ (LCMO) by mechanochemical processing [1,2], a process that makes use of chemical reaction activated by high-energy ball milling, and investigated their magnetic properties.

2. EXPERIMENTAL PROCEDURE

The starting materials used for the synthesis of LCMO nanopowders were $LaCl_3$, $CaCl_2$, $MnCl_2$ and Na_2CO_3 mixed in a molar ratio of 0.7 : 0.3 : 1 : 2.35, appropriate for the reaction $0.7LaCl_3 + 0.3CaCl_2 + MnCl_2 + 2.35Na_2CO_3 + 0.325O_2 \rightarrow La_{0.7}Ca_{0.3}MnO_3 + 4.7NaCl + 2.35CO_2$. A total of 4 g of the starting powder, together with twelve hardened-steel balls 9.5 mm in diameter, was loaded in a hardened-steel vial in an Ar-filled glove box and milled for 3 h in a SPEX 8000 mixer/mill. The as-milled powder was annealed in air at temperatures between 750 and 1200 °C followed by washing with deionised water to remover the NaCl by-product. The LCMO powders thus prepared were single-phase and had crystallite sizes (D) ranging between 24 nm and 1μm, depending on the annealing temperature [1].

Magnetic measurements were made on cold-pressed pellets 5 mm in diameter and about 0.7 mm in thickness using a SQUID magnetometer. The

Corresponding author: M. Muroi, e-mail: michihito@ant-powders.com

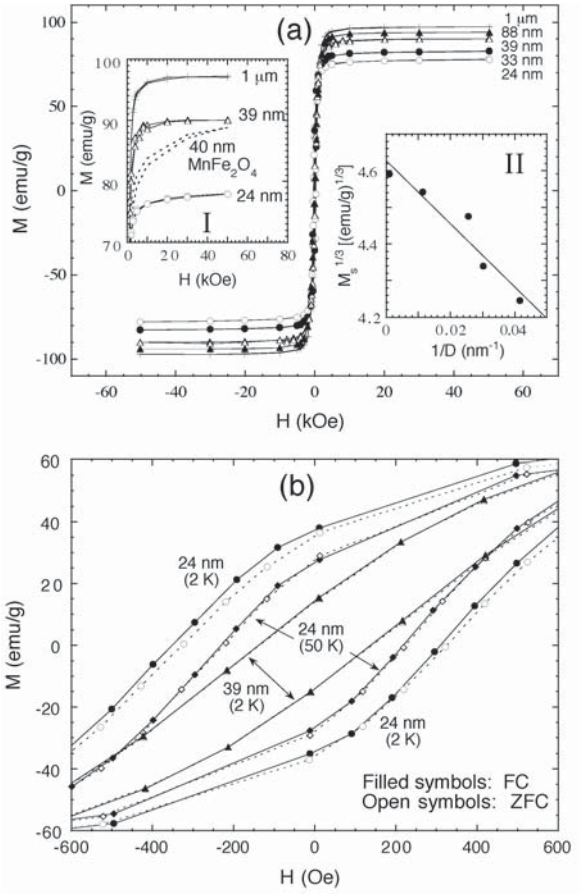

Fig. 1. (a) Hysteresis loops measured at 2K for LCMO particles having various values of *D*. Inset I: A large-*M* region shown with an expanded vertical axis. Data for 40-nm $MnFe_2O_4$ particles are included for comparison. Inset II: $M_s^{1/3}$ vs 1/*D* plot. (b) Low-field region of field-cooled (FC) and zero-field-cooed (ZFC) hysteresis loops for *D*=24 and 39 nm.

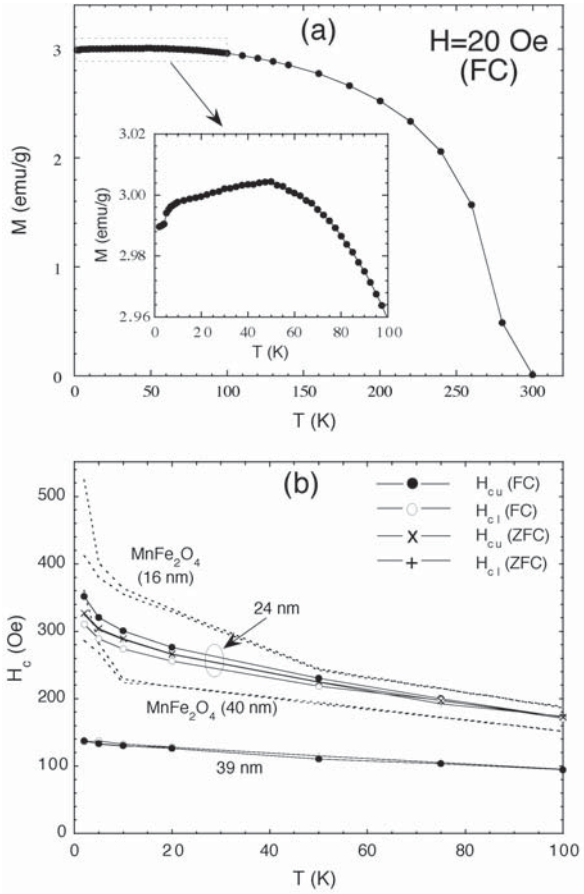

Fig. 2. (a) Temperature dependence of magnetisation measured in 20 Oe for 24-nm LCMO particles. (b) Temperature dependence of coercivity for 24- and 39-nm LCMO particles and for 16- and 40-nm $MnFe_2O_4$ particles. H_{cu} and H_{cl}, respectively, indicate coercivities for the upper branch (for decreasing field) and for the lower branch (for increasing field) of the hysteresis loop.

magnetic field was applied to the direction parallel to the flat surfaces of the pellet to reduce demagnetisation effects.

3. RESULTS AND DISCUSSION

In Fig. 1(a), field-cooled hysteresis loops measured at a temperature (*T*) of 2K are shown for various values of *D*. [Field-cooled (FC) and zero-field-cooled (ZFC) hysteresis loops are those measured after cooling the sample from room temperature in the maximum field (*H*) of 50 kOe and in zero field, respectively.] It is observed that the spontaneous magnetisation (M_s), determined by linear extrapolation of the data points for *H*>10 kOe to *H*=0, decreases with *D*; and that for smaller values of *D*, magnetic saturation is not complete even at 50 kOe. Both features are explained by assuming that each crystallite consists of a ferromagnetic core having a collinear spin configuration and a spin-glass shell having a disordered spin configuration [2,3]. The presence of a spin-glass shell, and not a paramagnetic shell, is evidenced by the *M* vs *T* curve measured in 20 Oe for the 24-nm particles [Fig. 2(a)], which exhibits a maximum at about 50K, a clear indication of spin freezing.

We can estimate the shell thickness (*t*), assuming that *t* is independent of *D* and *M*=0 for the shell. M_s will then vary with *D* as $M_s=M_{s0}(D-2t)^3/D^3$, or $M_s^{1/3} = M_{s0}^{1/3}(1-2t/D)$, where M_{s0} is the M_s for bulk LCMO. As can be seen in the inset II of Fig. 1(a), $M_s^{1/3}$ and

$1/D$ indeed show a reasonably good linear relationship, and from linear fit to the data points M_{s0} and t have been estimated to be M_{s0}=99.1 emu/g and t=0.93 nm. (The intercept at $1/D$=0 and the slope of the straight line correspond to $M_{s0}^{1/3}$ and $2tM_{s0}^{1/3}$, respectively.) The estimated shell thickness is very close to that for $MnFe_2O_4$ nanoparticles, 0.91 nm [2].

In a previous paper [1], we have ascribed the surface spin disorder in LCMO particles to the following two factors: (i) Mn atoms on the surface, having various oxygen coordination numbers, will have oxidation states different from those deep inside the bulk (~3.3), and (ii) the Madelung potential varies among Mn sites near the surface, resulting in localisation of e_g electrons. Under these circumstances, double-exchange interactions, which bring about ferromagnetism and metallic conductivity in optimally doped peroviskite manganites [4], give way to superexchange interactions, the sign of which depends on the oxidation states of neighbouring Mn ions and, when Mn^{3+} ions are involved, on the orientation of the occupied e_g orbitals [5]. Thus, positive and negative superexchange interactions coexist near the surface, causing frustration and hence spin disorder. Here, we suggest that perturbations to the crystal field, and the resultant surface anisotropy [2,3], are also responsible for the surface spin disorder. Deep inside a crystal, the crystal field at a Mn site has the same symmetry as the crystal structure, and so does the magnetocrystalline anisotropy. Near the surface, however, the atomic arrangement around a Mn site is not symmetric, providing perturbations to the crystal field. Although a crystal is electrically neutral as a whole, charge neutrality is not necessarily satisfied for each crystallographic plane, and charged surface layers set up roughly radial electric fields. Approximately radial, uniaxial anisotropy is thus created, leading to a noncollinear spin configuration near the surface.

In Fig. 2(b), the temperature dependence of coercivity (H_c) is shown for D=24 and 39 nm; H_c was determined for the FC and ZFC hysteresis loops, and H_c for both the upper and lower branches (H_{cu} and H_{cl}) are plotted. For D=39 nm, H_c is about 100 Oe and depends only weakly on temperature, and virtually no difference is observed between H_{cu} and H_{cl} or between H_c's for FC and ZFC. For D=24 nm, the temperature dependence of H_c is stronger than for D=39 nm at low temperature, and in the case of FC, H_{cu} becomes greater than H_{cl} below about 50 K. (For ZFC, H_{cu}=H_{cl} within experimental error, ~5 Oe.) These features are seen clearly in Fig. 1(b), where FC and ZFC hysteresis loops are shown for D=24 nm (T=2 and 50 K) and D=39 nm (T=2 K). For D=24 nm the FC hysteresis loop is shifted to the left at 2K, a characteristic of exchange-coupled systems [6], but the FC and ZFC hysteresis loops nearly coincide at 50K. For D=39 nm there is no difference between the FC and ZFC hysteresis loops even at 2K.

These observations are consistently explained in terms of a core-shell exchange-coupling model [2,3]. The spins in the shell, with multiple configurations, become frozen below the spin-freezing temperature (T_f) of ~50 K, making coherent rotation of the core spins more difficult. Cooling in a field establishes a shell-spin configuration favourable for the core magnetised in the direction of the field in which the sample is cooled, resulting in an exchange bias and hence a hysteresis-loop shift. These effects are stronger for a smaller particle because of a greater fraction of spins lying at the core-shell interface.

To visualise the magnetisation-reversal process in a LCMO nanoparticle, we have carried out Monte Carlo computer simulations based on a 3D Heisenberg model with classical spins. A Mn site in a peroviskite lattice was chosen as the origin, and approximately spherical crystals were generated by including all the Mn sites within a radius of $30^{1/2}a_0$, where a_0 is the lattice constant. The region within a radius of $12^{1/2}a_0$ from the origin was defined as the core, and the region outside it as the shell. This model system represents a crystal with D ~ 4 nm and t ~ 0.8 nm (~$2a_0$), containing a total of 739 spins. The Hamiltonian used for the simulation was

$$E = -\Sigma J_{ij}\boldsymbol{\sigma}_i\cdot\boldsymbol{\sigma}_j - S k_i \sigma_{z,i}^2 - S\boldsymbol{\sigma}_i\cdot\boldsymbol{H}, \quad (1)$$

where J_{ij} is the exchange interaction between nearest-neighbour (NN) spins $\boldsymbol{\sigma}_i$ and $\boldsymbol{\sigma}_j$ ($|\boldsymbol{\sigma}_i|$=1 for all i's); k_i the magnetocrystalline anisotropy constant; $\sigma_{z,i}$ the component of spin $\boldsymbol{\sigma}_i$ along the easy (z) axis; and $\boldsymbol{H}$ the magnetic field applied along the [001] axis. (The first, second and third terms of the right-hand side represent the exchange, anisotropy and Zeeman energies, respectively.) The following assumptions were made: (i) ferromagnetic exchange interactions (J_{ij}=J_F>0) for all the NN spin pairs within the core and across the core-shell interface; (ii) ferromagnetic (J_{ij}=J_F>0) or antiferromagnetic (J_{ij}=J_A<0) exchange interactions with an equal probability for the NN spin pairs within the shell; (iii) k_i=0 for the spins in the core; and (iv) radial uniaxial anisotropy for the spins within the shell. The parameters used were J_F=1, J_A=-1, k_i=0.05 (for shell spins) and T=0.01 [7]; these parameters are dimensionless

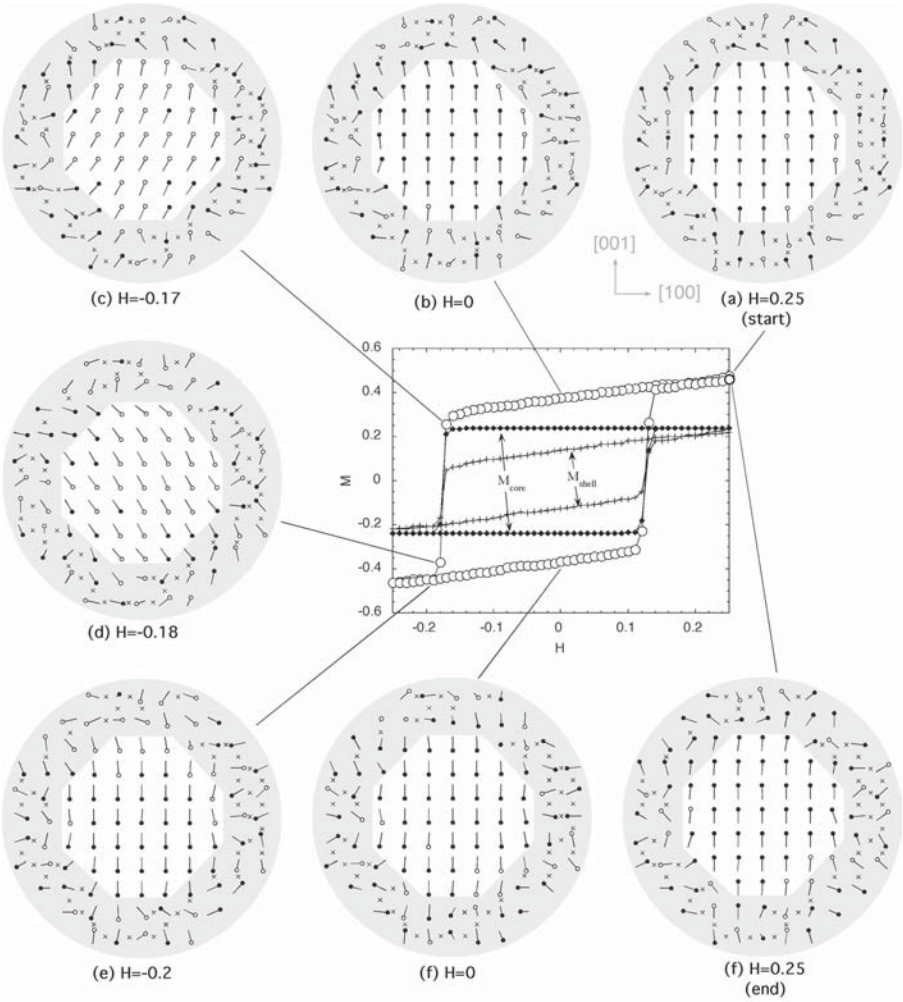

Fig. 3. Hysteresis loop obtained through a Monte Carlo computer simulation described in the text. M_{core} and M_{shell} indicate the contributions from the core and shell, respectively. (a-f) Configurations of the spins within the (010) plane at various points of the hysteresis loop. The spin vectors are projected onto the (010) plane so that a shorter bar denotes a spin making a larger angle with the (010) plane. The filled heads (•) indicate spins lying in the page or pointing out of the page, and the open heads (o), spins pointing into the page. The shaded area denotes the shell, and the crosses (x) indicate negative exchange interactions.

(normalised to J_F) and suitable for simulating low-temperature behaviour of a system having strong exchange interactions, weaker surface anisotropy, and negligibly weak bulk crystalline anisotropy. The simulations were carried out on a computer by progressively updating the spin configuration using a standard Metropolis algorithm. To obtain a hysteresis loop, H was cycled between 0.25 and -0.25 in steps of 0.01, and M was recorded after 2000 Monte Carlo steps had been performed at each value of H. (For the parameters chosen, the maximum field of 0.25 corresponds to about 69 kOe).

A hysteresis loop thus obtained is shown in Fig. 3; M is normalised to the value for full polarisation, and the contributions from the core (M_{core}) and the shell (M_{shell}) are also plotted. Lack of magnetic saturation and a hysteresis-loop shift towards negative H, two notable features of the FC hysteresis loop for D=24 nm at 2K (Fig. 1), are clearly observed. Except near H_c, $|M_{core}|$ is essentially constant at its saturated value of 0.242, and the H dependence of M arises almost entirely from that of M_{shell}. It is noted that magnetisation reversal in the core and shell take place at the same time because of exchange coupling.

Fig. 3(a-g) shows the spin configurations within the (010) plane at various points of the hysteresis loop. The spin vectors are projected onto the (010) plane so that a shorter bar denotes a spin making a larger angle with the (010) plane. The filled heads

(•) indicate spins lying in the page or pointing out of the page, and the open heads (o), spins pointing into the page. The shaded area denotes the shell, and the crosses (x) indicate negative exchange interactions. Examination of these diagrams provides further insight into the (de)magnetisation process:

Remanent magnetisation (M_r): It can be seen in Fig. 3 that most of the shell spins lying at the core-shell interface are oriented towards the direction of M_{core} regardless of field direction, thus making a significant contribution to the total M; for instance, M_{shell} accounts for 30% of M_r and 20-25% of the total M even at $H \sim H_c$. This is due to exchange coupling of the core and shell spins, which dominates the influence of applied field. Without exchange coupling, M_{shell} would be roughly linear in H and make little contribution to M_r.

Magnetisation reversal: As can be seen in Fig. 3(c-e), the core spins rotate coherently during magnetisation reversal. On the other hand, the shell spins tend to rotate in similar ways to the core spins, but the rotation is by no means coherent and there even exist groups of shell spins the configuration of which hardly changes during magnetisation reversal [e.g. a group of spins to the right of Fig. 3(c-e)]. Thus, coherent rotation of the core spins forces major changes in the shell-spin configuration, which require energy as different spin configurations in a spin glass are separated by a hierarchy of energy barriers. It is these energy barriers that prevent magnetisation reversal in the ranges $-H_{cu}<H<0$ (in the upper branch) and $0<H<H_{cl}$ (in the lower branch), where the total energy would be lowered if the magnetisation were reversed, i.e. the system is in a metastable state [8,9]. Above T_f, the energy barriers separating different shell-spin configurations are overcome by the thermal energy and the shell spins can always achieve an equilibrium configuration. The coercivity then arises only from the magnetocrystalline anisotropy, which is neglected in the simulation.

As we have reported in Ref. [2], $MnFe_2O_4$ nanoparticles exhibit properties very similar to those of LCMO nanoparticles described above. However, there are notable differences also evident as discussed below. (1) The increase in H_c with decreasing temperature and the hysteresis-loop shift at low temperature are much more pronounced for $MnFe_2O_4$ than for LCMO [see Fig. 2(b), in which the temperature dependence of H_c for $MnFe_2O_4$ nanoparticles is included], suggesting that the core-shell exchange coupling is much stronger in $MnFe_2O_4$ than in LCMO. This is ascribed to the fact that the density of magnetic ions is much higher in $MnFe_2O_4$ ($3.9 \cdot 10^{22}$ cm^{-3}) than in LCMO ($1.7 \cdot 10^{22}$ cm^{-3}) and, as a result, the number of pairs of magnetic ions interacting across the core-shell interface is much greater in the former than in the latter. (2) The slope of the hysteresis loop in a high-field region is much greater for $MnFe_2O_4$ than for LCMO [see inset I of Fig. 1(a)], indicating that the shell of a $MnFe_2O_4$ particle is magnetically much softer than that of a LCMO particle. This difference is elucidated, considering the origins of surface spin disorder in the two systems. In LCMO the surface spin disorder originates primarily in the partial replacement of ferromagnetic interactions with antiferromagnetic ones, and an energy comparable to J_A is needed to restore a collinear, ferromagnetic configuration. In $MnFe_2O_4$, by contrast, the surface spin disorder results primarily from imbalance in the numbers of ferromagnetic and antiferromagnetic bonds, and from modifications to the magnitude of exchange interactions [2]. Since no change in the sign of exchange interaction is involved, a relatively low energy, much lower than the exchange energies themselves, is needed to restore a collinear, ferrimagnetic configuration.

4. CONCLUSIONS

Nanoparticles of $La_{0.7}Ca_{0.3}MnO_3$ have been synthesised by mechanochemical processing and their magnetic properties investigated. It was found that the spontaneous magnetisation decreased with crystallite size (D); and that for the smallest particles (D=24 nm) below about 50K, the field-cooled hysteresis loops were shifted towards negative field and the coercivities increased sharply with decreasing temperature. These observations are consistently explained in terms of a model in which it is assumed that each crystallite consists of a ferromagnetic core and a spin-glass shell that are coupled through exchange interactions.

REFERENCES

[1] M. Muroi, R. Street and P. G. McCormick // *J. Appl. Phys.* **87** (2000) 3424.
[2] M. Muroi, R. Street and P. G. McCormick // *Phys. Rev. B* **63** (2001) 184414.
[3] R. H. Kodama and A. E. Berkowitz // *Phys. Rev. B* **59** (1999) 6321.
[4] J. M .D. Coey, M. Viret and S. von Molnár // *Adv. Phys.* **48** (1999) 167.
[5] J. B. Goodenough, *Magnetism and the Chemical Bond* (Interscience, New York, 1963).
[6] J. Nogués and I. K. Schuller // *J. Magn. Magn. Mater*. **192** (1999) 203.

[7] Eq. (1) in conjunction with these parameters is equivalent to the complete Hamiltonian $E=-\Sigma J_{ij}\boldsymbol{S}_i\bullet\boldsymbol{S}_j - \Sigma k_i S_{z,i}^2 - \Sigma g\mu_B \boldsymbol{S}_i\bullet\boldsymbol{H}$ with $|\boldsymbol{S}_i|=S=1.85$, J_F=20K, J_A=-20K, k_iS^2=3.4K and T=0.68K. These parameters roughly reflect those determined experimentally for peroviskite manganites (Ref.[4]).

[8] The total exchange energy ($E_J=-\Sigma J_{ij}\boldsymbol{\sigma}_i\bullet\boldsymbol{\sigma}_j$) was calculated at each value of H during the simulation. The E_J vs H plot thus obtained indeed showed sharp peaks near $H=\pm|H_c|$.

[9] Finite, if weak, anisotropy is needed for this coercivity mechanism to be operative; without one, all the spins would rotate coherently in an infinitesimally low negative field.